Journal of Materials Chemistry C

Photochemical Phase and Alignment Control of a Nematic Liquid Crystal in Core-Sheath Nanofibers

Journal:	*Journal of Materials Chemistry C*
Manuscript ID	TC-ART-05-2021-002392.R1
Article Type:	Paper
Date Submitted by the Author:	28-Jul-2021
Complete List of Authors:	Thum, Matthew; US Naval Research Laboratory Ratchford, Daniel; US Naval Research Laboratory Casalini, Riccardo; US Naval Research Laboratory, Chemistry Division Kołacz, Jakub; US Naval Research Laboratory, Center for Bio/Molecular Science and Engineering Lundin, Jeffrey; US Naval Research Laboratory, Department of Chemistry

ARTICLE

Photochemical Phase and Alignment Control of a Nematic Liquid Crystal in Core-Sheath Nanofibers

Received 00th January 20xx,
Accepted 00th January 20xx

DOI: 10.1039/x0xx00000x

Matthew D. Thum[a,†], Daniel C. Ratchford[a], Riccardo Casalini[a], Jakub Kołacz[b], Jeffrey G. Lundin[a,*]

Electrospinning serves as a versatile means of understanding the effects of strong cylindrical confinement on encapsulated liquid crystals (LCs) and is a promising technique for developing functional fabrics and surfaces. In this work, we use electrospinning to create core-sheath nanofibers composed of a polyvinylpyrrolidone (PVP) sheath doped with a photochromic, azobenzene-based surfactant, and a low-molecular weight nematic liquid crystal core. The incorporation of an azobenzene surfactant into the polymer sheath allows for photochemical control over the nematic to isotropic transition temperature of the LC core resulting in ultra violet (UV) irradiation-induced depression of the phase transition temperature. Owing to the photochromic nature of the surfactant, the photoinduced decrease in the transition temperature is reversed with visible light irradiation with no notable fatigue resistance. At high surfactant loading rates, the temperature of the photoinduced phase transition is reduced to below room temperature allowing for the birefringence of the nanofibers "on" and "off" with irradiation and requires no external heating. Based on these oberservations, we propose photoisomerization of the azobenzene-based surfactant at the PVP/LC interface leads to surface induced disorder of the LC core changing the orientation from planar axial to random with UV irradiation and reversing that change with visible irradiation. This is further substantiated by examinig the LC alignement within nanofibers by imaging the fibers with the addition of a quarter-wave retardation plate. This method adds to the growing set of tools available for the control of the phase behavior of encapsulated liquid crystals and expands the functionality of electrospun materials.

Introduction

The ability to modulate the optical properties of liquid crystalline materials (i.e. alignment, phase behavior) underpins all LC-based technology. Some methods to induce LC alignment include molecular surface design with Langmuir Blodgett films[1-3], monolayer self-assembly[4], and with the addition of nanoparticle dopants.[5-7] However, the drive to develop a spatially directed, contact-free method to control LC optical properties has led to the use of photochemistry as a tool to affect LC behavior.[8, 9] Photochemistry allows for spatial and temporal control over a given chemical reaction making it a powerful tool for the localized control frequently needed for "smart" materials and sensors. The ability to photochemically control the optical properties of LCs has been demonstrated with photochromic molecules such as spiropyran[10], fulgide[11], and azobenzene.[9, 12]

Since the first report of the *cis*-isomer of Azobenzene in 1937, it has been the subject of extensive study and its applications have been highlighted in multiple review articles.[9, 13-17] Azobenzene is an ideal photoswitch for possible applications due to its fast, reversible, and efficient photoisomerization and broad separation of isomeric absorption spectra allowing for the selective irradiation of either isomer leading to a high concentration of photoproduct in the photostationary state.[16, 18-21]

Extensively studied by the Ikeda group, the rod-shaped *trans*-azobenzene is compatible with the bulk of nematic LCs. Photoisomerization of azobenzene, however, leads to the formation of the bent-shaped, *cis* isomer which is broadly incompatible with the LC matrix.[22-26] This was most commonly used in "command surfaces" of Langmuir Blodgett films containing azobenzene moieties which have been extensively studied for photoaligment.[27-30] Additionally, azobenzene and its derivatives have been used as dopants to grant photochemical control over phase behavior in liquid crystals.[12, 22-25, 31-33] Aside from traditional command surfaces, alignment control in liquid crystalline polymers has also been recently demonstrated by grafting azobenzene moieties onto gold nanoparticles for use as dopants in LC mixtures.[34]

In addition to external stimuli (i.e. light, heat), confinement has proven an effective method of controlling LC alignment and phase behavior.[35, 36] Electrospinning can be used to fabricate a broad range of nonwoven fibers and yarns with varying properties and morphologies, and coaxial electrospinning has proved a versatile method of investigating confinement of LCs within micro- and nano-scale cylindrical geometries.[35-40] The morphology of the fibers is affected by many parameters including flow rate, applied voltage, distance from the spinneret

[a] *Chemistry Division, Naval Research Laboratory, 4555 Overlook Avenue SW, Washington, D.C. 20375*
[b] *Center for Bio/Molecular Science and Engineering, Naval Research Laboratory, 4555 Overlook Avenue SW, Washington, D.C. 20375*
† American Society for Engineering Education Post-Doctoral Research Associate
Electronic Supplementary Information (ESI) available: [details of any supplementary information available should be included here]. See DOI: 10.1039/x0xx00000x

tip to the collector, and relative humidity.[41, 42] In coaxial electrospinning, a small (inner) needle is inserted within a larger (outer) needle and two solutions are pumped through the system so that the outer solution encompasses the inner solution at the Taylor cone formed at the needle tip. The resulting fibers have a core-sheath morphology in which the inner compound is completely encompassed by a sheath made up of the remains of the evaporated outer solution. Encapsulated LCs fabricated by electrospinning have been used as flexible temperature[43, 44] and gas[45, 46] sensors, and have been fabricated with multiple cores for additional variability of stimuli response.[39] Additionally, azobenzene moieties have been incorporated into LC core nanofibers for color tunability[47] and photoimaging.[48]

Electrospinning has also been shown to increase the effects of topological constraints due to the small-scale confinement of the LC within the nanofiber core.[35] It has been previously observed that the incorporation of surfactants into the sheath solution can lower viscoelasticity resulting in defect-free fibers.[49] Furthermore, the addition of surfactants into the polymer sheath has been demonstrated as a facile method to control LC ordering within electrospun nanofibers.[50] Surfactants have long been used in confined systems to induce LC alignment along a surface by promoting either planar (parallel) or homeotropic (perpendicular) alignment. Properties such as alkyl chain length, surfactant density along the surface, and temperature can all have significant effects on the surface orientation of LC.[51]

This work builds upon the confinement effects of electrospun LCs in polymeric sheaths, the photochemical control of azobenzene "command surfaces", and the LC alignment control of surfactants. Herein, we describe a system in which an azobenzene-based surfactant is incorporated into the polymeric sheath encompassing a nematic LC core in electrospun nanofibers creating a system where the LC core in the resultant core-sheath nanofibers is responsive to temperature, UV/Visible irradiation and confinement. Irradiation with UV light is shown to decrease the nematic to isotropic transition temperature ($T_{N\rightarrow I}$) of the LC core due to increased disorder present at the LC/polymer interface, and, at the highest concentration of photochromic surfactant used, the birefringence of the LC was able to be turned "on" and "off" photochemically at, or below, room temperature. This work presents the first example of using the increased surface effects on confined liquid crystals as a means to photochemically control the phase behavior of an encapsulated liquid crystal within a flexible, polymeric, nanofiber and opens the possibility for the incorporation of photoresponsive fibrous mats into flexible, electrospun "smart" materials[52-55] and surfaces.[56-58]

Materials and Methods

Materials. Unless otherwise noted, all chemicals were provided by Sigma Aldrich. Polyvinylpyrrolidone (PVP) (M_w 1,300,000 g/mol) was obtained from Acros Organics, 4-Cyano-4'-n-pentylbiphenyl (**5CB**) was obtained from TCI America, Ethanol was obtained from The Warner-Graham Company, and Sodium Chloride was obtained from Fisher Scientific. The synthesis of **C_4AzoC_6PEG** is detailed in the Supporting Information. All materials were used as received.

Solution Preparation. PVP was dissolved in 90/10 ethanol/water at 12.5 wt% with 0.05 wt% NaCl and 0-3.0 wt% **$C_4AzoC_6PEG_3$**. **5CB**, a nematic LC, was used neat as the core solution. The addition of NaCl aimed to increase the electrical conductivity of the solution to promote the formation of thinner fibers.

Electrospinning. Coaxial electrospinning was performed on a custom-built apparatus utilizing two New Era Syringe Pumps (NE-300). The syringe pumps were equipped with a 1 mL syringe containing the neat 5CB fixed with a coaxial needle (Ramé-Hart, inner Gauge 22/outer Gauge 12) and the other with a 12 mL syringe containing the PVP/**$C_4AzoC_6PEG_3$** sheath solution connected to the outlet of the coaxial needle through Tygon tubing. The needle was set at distance of 14 cm away from the collector horizontally. The voltage between the needle and collector was set to 10.5-13.5 kV by a Matsusada high voltage power supply. The syringe pump flow rate was 0.5 mL•hr^{-1} for the core and was held constant at 3.00 mL•hr^{-1} for the sheath solution. Fibers were collected onto aluminum foil, glass slide, or SEM post. Fibers were analyzed within 24 hours of spinning. Uniform, defect free, fibers were obtained after spinning in a fume hood at 18 – 23 °C and a relative humidity of 10 – 35%.

Polarized Optical Microscopy (POM). Polarized optical microscopy was performed using a Zeiss Axio Imager 2 equipped with cross-polarizers. Images were taken using EC Epiplan-Neofluar 5−100× objectives and processed using Zen Core software (Zeiss, Oberkochen, Germany). Samples were prepared on glass slides and were analyzed in reflection or transmission mode, respectively, under both polarized and 90° cross-polarized light. The microscope was also equipped with a Linkam PE120 thermal stage, with which the temperature was controlled from room temperature to 37 °C at a rate of 1 °C•min^{-1} to observe phase transitions. Fiber dimensions were measured from POM images using Image J software (n ≥ 100)

Photolysis. Samples were irradiated using an Omnicure Series 2000 from Lumen Dynamics with either 365, or 400-500 nm filters. The light was guided through a fiber optic cable and the samples were irradiated at distance of approximately 10 cm for less than 5 seconds. The irradiation intensity was 100 mW•cm^{-2} for all experiments.

UV/Vis Spectroscopy. UV-Vis spectra were obtained on an Agilent 8453 UV-Visible spectrophotometer, with a spectral range of 190 - 1100 nm, and subsequently analyzed with Chemstation software.

Scanning Electron Microscopy (SEM). SEM was performed on a JEOL JSM-7600F field emission scanning electron microscope (Peabody, MA) operated at an accelerating voltage of 3 kV equipped. Samples were sputter-coated with least 3 nm gold prior to SEM analysis using a Cressington 108 autosputter coater equipped with an MTM20 thickness controller. ImageJ software was utilized to measure fiber sizes from the SEM images.

Focused Ion Beam - Scanning Electron Microscopy (FIB-SEM). Fibers were milled with a FEI Helios focused ion beam scanning electron microscope. Immediately after milling, cross sectional

scanning electron microscopy images of the fibers were acquired with the same FEI Helios system.

Differential Scanning Calorimetry (DSC). TA Instruments Discovery DSC (New Castle, DE) was employed to investigate the phase transitions of the core-sheath fibers. Samples were cut from the electrospun mat and placed into Tzero Pans (TA Instruments). The DSC equilibrated at 5 °C before a temperature ramp to 60 °C at a rate of 5 °C•min^{-1}. The sample was then cooled at a rate of 5 °C•min^{-1} to 10 °C. This process was repeated three times. Results were analyzed using TA Instruments TRIOS software.

Results and Discussion

Surfactant Design and Synthesis.

A general description of the compounds used in this study is given in Figure 1. Azobenzene-based surfactants are composed of an aliphatic tail, a photoactive core, and a polar head group. Previous work has shown that azobenzene-based surfactants affect the $T_{N\rightarrow I}$ when added as dopants to a nematic LC matrix. Depending on the nature of the substituents and the structure of the photoactive core, azobenzene-based surfactants have been observed to have both a positive and a negative effect on the order parameter in a nematic LC[32, 59]. In this work, **$C_4AzoC_6PEG_3$** was designed to have a short-chain aliphatic tail to minimally disrupt LC ordering while at the polymer/LC interface.[50] Additionally, a short polyethylene glycol (PEG) chain was used as the polar head group to aid in solubility in the PVP polymer solution and promote favorable PVP/surfactant interactions in the nanofibers. A low molecular weight nematic LC, **5CB**, was used as the core solution because it's crystalline to nematic (Cr → N) temperature lies below room temperature aiding in electrospinning without the need for external heating. Finally, PVP was used as the polymer sheath due to its solubility

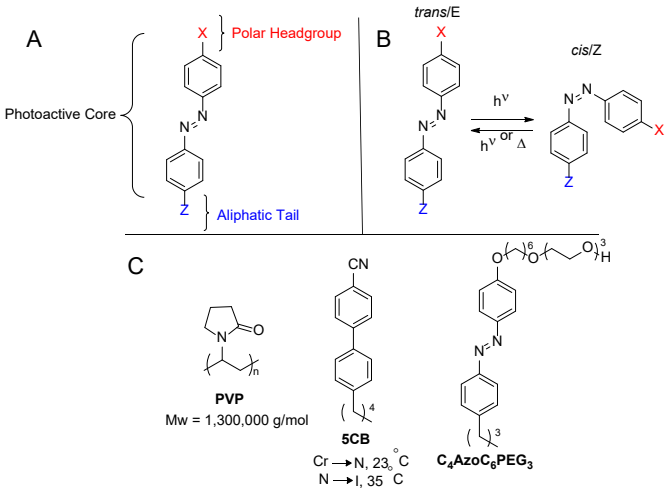

Figure 1. (*A*) Design of photochromic surfactant, **$C_4AzoC_6PEG_3$**. The surfactant comprises an aliphatic tail, a photoactive core, and a polar headgroup. (*B*) When in its *trans* form, the surfactant is rod-shaped and does not significantly disrupt LC ordering. However, in its *cis* form, **$C_4AzoC_6PEG_3$** is bent-shaped and is incompatible with the LC matrix. (*C*) The structure of the rod-shaped, low molecular weight, nematic LC, **5CB** ,and relevant properties and structures of the compounds used in this work.

in ethanol and availability in high molecular weight. In acetonitrile at room temperature, **$C_4AzoC_6PEG_3$**, exists primarily in it *trans* isomer and has a strong absorption band at 365 nm and a weaker band stretching out to ca. 425 nm. Upon irradiation, **$C_4AzoC_6PEG_3$** undergoes rapid *cis* – *trans* isomerization which can be seen in the UV/Visible spectra as a growth of a new peak at ca. 450 nm and the loss of the peak at 365 as it blue-shifts to a weaker signal at ca. 300 nm (Figure S-5). In solution at 365 nm, *cis* – *trans* isomerization was rapid, with the photostationary state being reached in less than 10 seconds of irradiation. The lifetime of the *cis* isomer was calculated by measuring the recovery of the *trans* isomer in the dark and fitting the recovery to a first order kinetic model (Figure S-6). In acetonitrile at room temperature, the *trans* isomer of **C_4AzoC_6PEG** has a half-life ($t_{1/2}$) of ca. 20.3 hours. Photolysis of the *cis* isomer with 400-500 nm visible light results in the recovery of the peak at 348 nm, reforming the *trans* isomer and demonstrating the photochromic nature of the isomerization (Figure S-5).

Nanofiber Fabrication

Monofilament fibers were electrospun from 12.5 wt% PVP solutions in 90/10 ethanol/water mixtures containing up to 3.0 wt% of **$C_4AzoC_6PEG_3$** and 0.05 wt% NaCl. Uniform fibers were observed containing up to 3 wt% of **$C_4AzoC_6PEG_3$** with no adverse effects of the incorporation of the surfactant on the fiber morphology (Figure S-4). Once it was determined that the addition of the surfactant into the PVP polymer sheath solution did not have a detrimental effect on the electrospinning process, nanofibers were electrospun using a coaxial needle setup (Ramé-Hart, inner Gauge 22/outer Gauge 12) using PVP containing 0 - 3.0 wt% of **$C_4AzoC_6PEG_3$** as the sheath and neat **5CB** as the core solution. Fibers were spun onto aluminum foil or glass slides at an applied voltage of 10.5 - 13.5 kV oriented 14 cm horizontally from the spinneret tip. The flow rate of the core solution and sheath solution was held constant at 0.5 mL•hr^{-1} and 3.0 mL•hr^{-1} respectively. SEM was used to examine fiber morphology and FIB-SEM was used to mill out sections to confirm core-sheath geometry.

Upon heating above the $T_{N\rightarrow I}$, the birefringence of the LC disappears as the LC core becomes isotropic (Figure 2, A-B). Upon cooling below the $T_{N\rightarrow I}$, the birefringence of the LC returns as the core becomes nematic suggesting that the nanofibers maintain core-sheath morphology as the LC is behaving similar to bulk (Figure 2, Figures S-9 – S-11). An example of thermally and photochemically induced N → I phase transition is shown in Figure 2. Figure 3 shows the nematic to isotropic transition temperature ($T_{N\rightarrow I}$) of nanofibers manufactured with 0 – 3 wt% of **$C_4AzoC_6PEG_3$** before and after UV irradiation. Before irradiation, the incorporation of **$C_4AzoC_6PEG_3$** into the polymer sheath results in a decrease in the $T_{N\rightarrow I}$ of the **5CB** core which has been previously attributed to a disruption of the cyano-PVP surface anchoring with the polar head of the surfactant orienting with the PVP backbone and the hydrophobic tail orienting itself towards the LC core.[50]

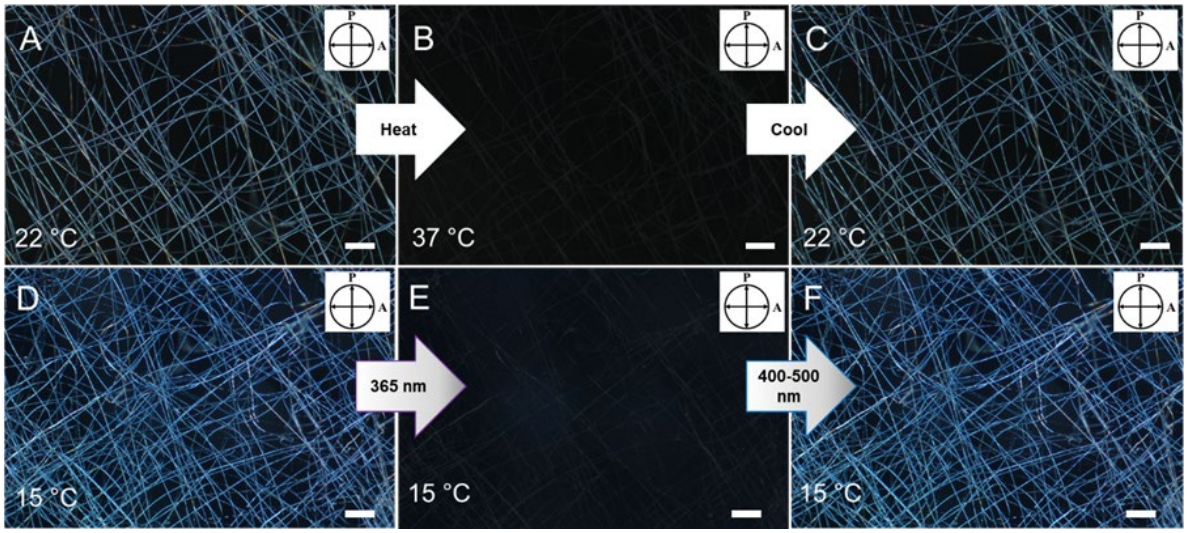

Figure 2. Crossed POM images showing reversible, photochemical depression of the $T_{N\rightarrow I}$ of **5CB**. Fibers are shown with 3 wt% **$C_4AzoC_6PEG_3$**. Scale Bars are 50 µm. *A-C* shows the loss of birefringence of the **5CB** core from thermally induced N → I transition when heating the sample above 35 °C. *D-F* Shows the reversible, photochromic, N → I transition at 15 °C. At these temperatures, UV (365 nm) light causes the **5CB** to become completely isotropic while visible (400-500 nm) irradiation causes the sample to transition back to the nematic phase.

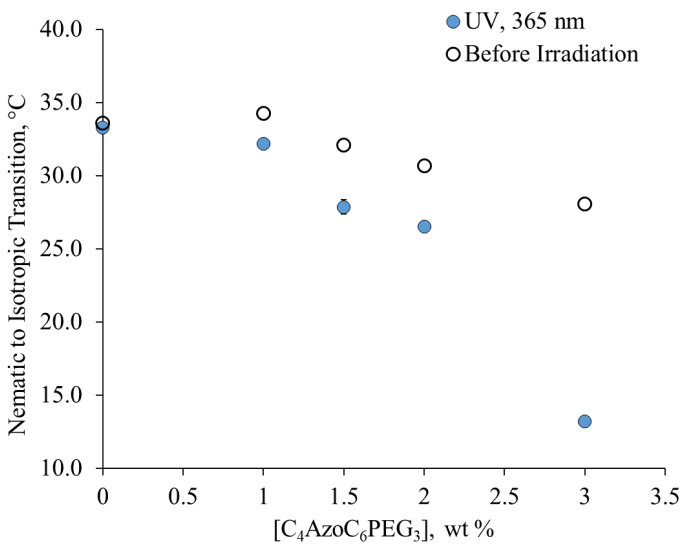

Figure 3. $T_{N\rightarrow I}$ of coaxial electrospun fibers containing a **5CB** core and a PVP sheath with 0-3 wt% of **$C_4AzoC_6PEG_3$**. The phase transitions were identified by the loss of birefringence of the LC core and error bars are the result of triplicate measurements. The transition temperatures were measured before (as spun) and after UV irradiation at 365 nm for 5 seconds.

After UV irradiation, there is a significant depression of the $T_{N\rightarrow I}$ which is amplified with an increase in the concentration of **$C_4AzoC_6PEG_3$**. Control experiments performed in the absence of surfactant show no change in $T_{N\rightarrow I}$ with UV irradiation. At relatively low concentrations (i.e. 1.0, 1.5 wt%) of surfactant, there is a small ca. 2 °C change in the transition temperature with UV irradiation. However, at 3.0 wt% of **$C_4AzoC_6PEG_3$**, the $T_{N\rightarrow I}$ significantly drops from 28.1 to 13.1 °C allowing for the photoinduced loss of birefringence to be observed at or below room temperature (Figure 2 D-F). In all cases involving the photochromic surfactant, visible light irradiation causes the LC to return to the initial, pre-irradiated, state suggesting isomerization of **$C_4AzoC_6PEG_3$** as the operative mechanism in the $T_{N\rightarrow I}$ depression. The process of photoinduced phase transition can be repeated multiple times without noticeable fatigue resistance (Figure S-8). Surfactant present at the LC/polymer interface in its *trans* form slightly disrupts the ordering of the core LC, however, upon UV irradiation, any *cis* photoproduct formed at the interface significantly decreases the LC ordering due to the incompatibility of the bent *cis* isomer with the rod-shaped LC.

Fiber Morphology

Incorporation of the photochromic surfactant into the polymer sheath leads to a decrease in the fiber diameter while still maintaining uniform, cylindrical morphology. In the absence of added surfactant, the PVP-**5CB** fibers had an average outer diameter of 1.72 ± 0.26 µm while adding only 1.0 wt% of $C_4AzoC_6PEG_3$ resulted a decrease in the outer fiber diameter to 1.38 ± 0.18 µm. At 3.0 wt% of surfactant, outer fiber diameters measured 1.29 ± 0.18 µm and nanofibers became less uniform with more observable flattened or evacuated areas (Figure 4). However, as can be clearly seen in Figure 4, FIB-SEM images show core-sheath morphology was maintained up to 3.0 wt% without compromising the core-sheath integrity. A decrease in outer fiber diameter with the addition of surfactant is consistent with previous observations that the presence of surfactants in the polymer sheath in electrospinning can lead to a change in the surface/interfacial tension and thus the spinning parameters.[49]

Images of the fiber core taken with FIB-SEM allow for a direct measurement of the core dimensions. The inner-core diameter varied significantly with fiber diameter and was measured between 0.6 – 1.1 µm across all fiber samples. As fiber diameters were statistically similar between samples made with 1.0 and 3.0 wt% **$C_4AzoC_6PEG_3$** (Table 1), the

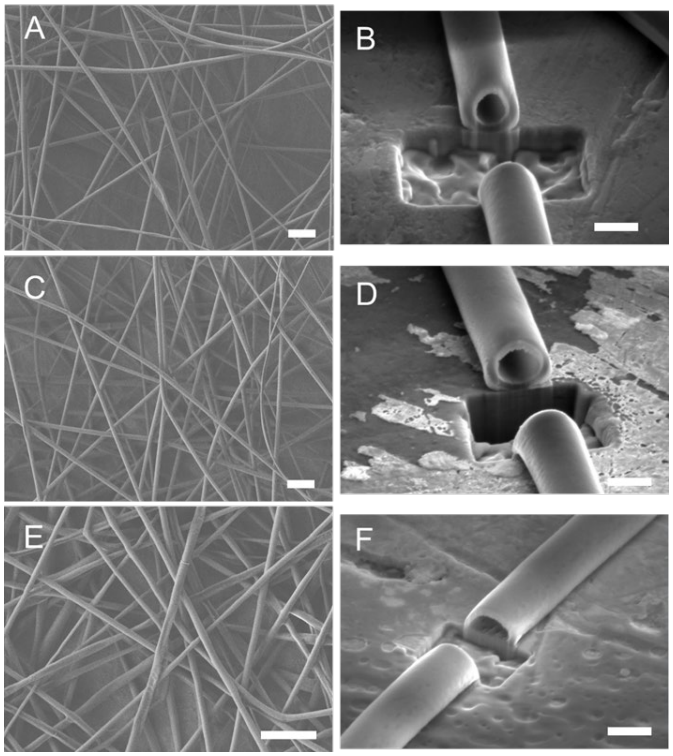

Figure 4. SEM images of nanofibers made with 0 wt% (A, B), 1.5 wt% (C, D), and 3 wt% (E, F) of **$C_4AzoC_6PEG_3$**. FIB-SEM images showing milled out sections of the fibers revealing the core-sheath morphology. Scale Bars: A, C, E = 10 µm; B, D, F = 1 µm.

Table 1. The effect of the concentration of $C_4AzoC_6PEG_3$ on fiber morphological and optical properties

[$C_4AzoC_6PEG_3$], wt%	Fiber diameter, µm[a]	$T_{N\rightarrow I}$ °C[b]	$T_{N\rightarrow I,\ UV}$ °C[b]	$\Delta T_{N\rightarrow I}$
0.0	1.72±0.26	33.6±0.2	33.3±0.2	0.3±0.1
1.0	1.38±0.18	34.3±0.2	32.2±0.1	2.1±0.2
1.5	1.39±0.17	32.1±0.4	27.9±0.6	4.2±0.5
2.0	1.24±0.14	30.7±0.6	26.5±0.2	4.2±0.4
3.0	1.29±0.18	28.1±0.2	13.2±0.1	14.9±0.2

[a] Average of ≥ 100 measurements. [b] Error bars as a result of triplicate measurements

significant decrease in $T_{N\rightarrow I}$ seen only in 3.0 wt% **$C_4AzoC_6PEG_3$** fibers was primarily attributed to surfactant concentration effects independent of fiber diameter. In coaxial electrospinning, core-sheath nanofibers can only be formed when the two solutions are immiscible enough to enable both the inner and out jets to stretch at the same rate.[42] Importantly, this demonstrates that the presence of **$C_4AzoC_6PEG_3$** within the polymer sheath solution did not have a significant effect on the diffusion of the LC into the polymer solution in the Taylor cone during electrospinning, and that the observed photochemical response is primarily a result of interactions that take place at the core-sheath interface. A summary of morphological and optical properties from the fibers fabricated in this study is shown in Table 1.

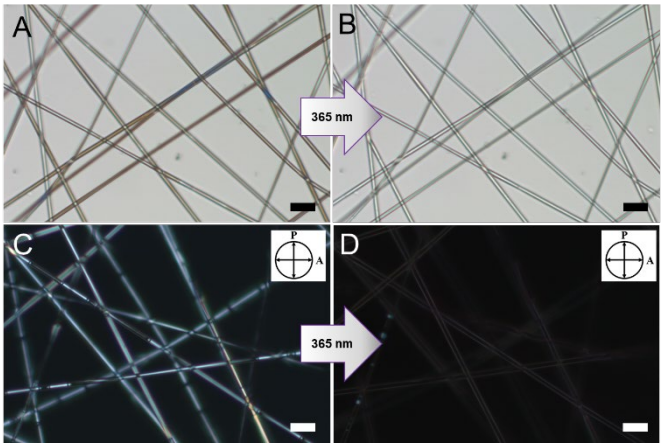

Figure 5. POM images of 1.5 wt% **$C_4AzoC_6PEG_3$** at 25° C before (*A, C*) and after (*B, D*) UV irradiation. Images A and B were taken using polarized light illumination and images C and D were taken under crossed polarizers. Scale bars = 10 µm.

The non-destructive nature of the irradiation is demonstrated in Figure 5. Although UV irradiation causes a depression of the $T_{N\rightarrow I}$, no morphological changes are observed before, during, or after irradiation. POM images of fibers are shown before (Figure 5 A) and after (Figure 5 B) UV irradiation and, aside from the change in birefringence associated with a disordering of the LC core (Figure 5 C and D), there is no morphological change in the properties of the nanofibers even after multiple "on"/"off" cycles of photolysis.

Liquid Crystal Alignment

When confined in cylindrical geometries, LC's can exhibit planar (parallel) or homeotropic (perpendicular) orientation due to surface interactions at the surface/LC interface as well as defects that change orientation within the bulk LC core.[35, 36] Previous work using polarized 2-D Raman spectroscopy has shown a nematic LC has planar, or escaped radial, orientation in the core of coaxial electrospun PVP nanofibers.[40] Additionally, it has been shown that the presence of surfactants within the PVP polymer sheath help reduce planar surface anchoring and induce interface localized homeotropic alignment along the polymer/PVP boundary.[50] In our system, alignment of the liquid crystals within the polymer nanofibers was investigated using crossed POM with the addition of a quarter-wave retardation plate to determine to what degree the presence of **$C_4AzoC_6PEG_3$** affects LC alignment (Figures 6 and 7). An example of using a quarter-wave retardation plate to investigate LC alignment is shown in Figure 6.

The use of a quarter wave retardation plate in POM allows for the visualization of the interference colors that result from polarized light moving through the liquid crystal core as they are oriented along their fast (yellow) and slow (blue) optical axis. The color gradient seen in a continuous, curved fiber shown in Figure 6 demonstrates that the LC is aligned along the fiber long axis as the color can been seen gradually changing from blue to yellow as the LC director is changing with the curve of the fiber.

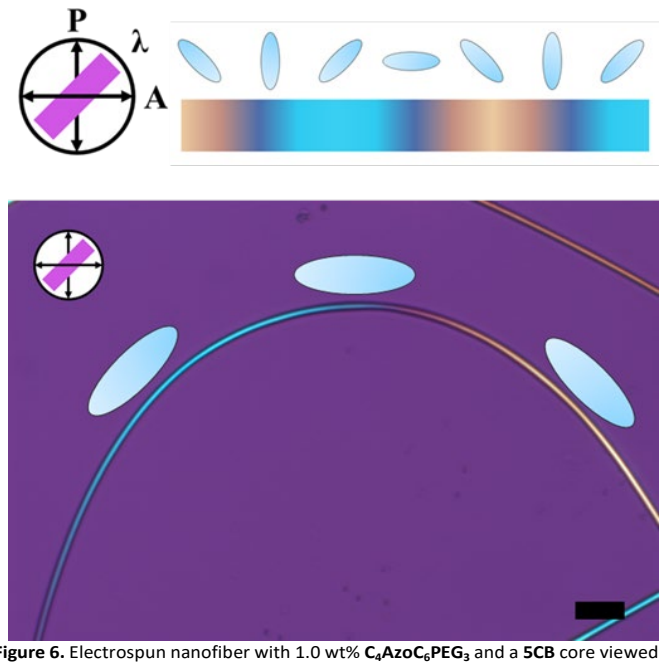

Figure 6. Electrospun nanofiber with 1.0 wt% **$C_4AzoC_6PEG_3$** and a **5CB** core viewed with crossed POM and quarter-wave retardation plate showing axial planar alignment of the LC within the fiber. Color bar at top depicts how the image color corresponds to the LC orientation. Color change along the fiber indicates that the LCs are aligned along the fiber long axis. Scale bar = 10 µm.

In the absence of surfactant, **5CB** shows strong axial planar alignment along the fiber long axis (Figure 7A). Although there are small defects present in the LC orientation, the director of the LC core is primarily ordered parallel with the fiber long axis with no observable defects at the interface. At up to 1.5 wt% of **$C_4AzoC_6PEG_3$**, there is no observed deviation from axial planar alignment (Figure 7B). The presence of small amounts of *trans*-surfactant at the core-sheath interface are not expected to significantly affect the LC ordering and surface anchoring of **5CB** at the polymer/LC interface. These observations are consistent with the measured $T_{N\rightarrow I}$ before irradiation at 1.0 and 1.5 wt% of **$C_4AzoC_6PEG_3$** given in Table 1. In contrast, at 3.0 wt% of **$C_4AzoC_6PEG_3$**, there are periodic changes in the LC orientation along the fiber axis which is broadly consistent with disorder of the **5CB** core induced by the increased concentration of surfactant (Figure 7C). Although *trans*- **$C_4AzoC_6PEG_3$** is not expected to significantly alter bulk LC order, its existence at high concentrations at the polymer/LC surface may disrupt strong **5CB**/PVP surface anchoring leading to a less-ordered LC core. This, too, is evidenced by the N → I transition before irradiation as 3.0 wt% drops the transition temperature by ca. 5 °C when compared to the control. Although the LC core in fibers made with 2.0 and 3.0% of **$C_4AzoC_6PEG_3$** shows a decrease in LC order, fibers made at these concentrations are still brightly birefringent (Figures S-16 and S-17) and the disorder induced by the presence of **$C_4AzoC_6PEG_3$** at the surface contributes beneficially to the large depression of the $T_{N\rightarrow I}$ observed in these systems and the ability to photochemically control the phase behavior without external heating.

Figure 8 shows POM images taken with a quarter-wave retardation plate of nanofibers made with 1.5 wt% of

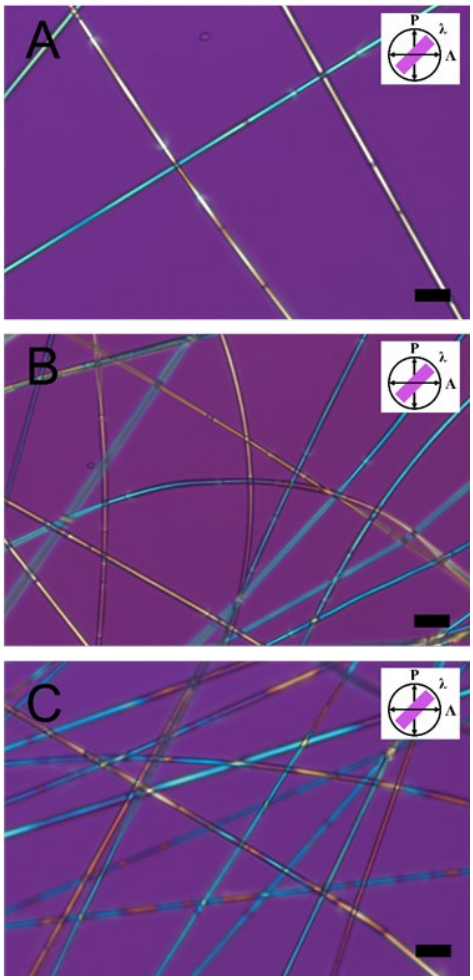

Figure 7. POM images of electrospun fibers viewed with a quarter-wave retardation plate. *A.* 0.0 wt% **$C_4AzoC_6PEG_3$** *B.* 1.5 wt% **$C_4AzoC_6PEG_3$** *C.* 3.0 wt% **$C_4AzoC_6PEG_3$**.

$C_4AzoC_6PEG_3$ demonstrating the effect of UV irradiation on the order of the **5CB** core. At temperatures above the $T_{N\rightarrow I}$, UV irradiation induces significant disorder in the LC core. Although, at these experimental temperatures, irradiation does not cause the $T_{N\rightarrow I}$ of the LC to drop below the experimental temperature (Figure 8, Experimental temperature = 23 °C, $T_{N\rightarrow I,\ UV}$, 1.5 wt% **$C_4AzoC_6PEG_3$** = 27.9 ± 0.6 °C, from Table 1), significant disorder in the LC core can be seen as the LC core loses all significant axial planar alignment.

As the concentration of **$C_4AzoC_6PEG_3$** is increased, the endorthermic N → I transition decreases in temperature and the peak becomes broader as observed by DSC (Figure S-19). Both the shift to lower temperatures and the broadening of the peak associated with the N → I transition are indicitave of a less-stable, more-disordered, LC core due to disruption of the surface anchoring ability of **5CB** with the polymer sheath.

The results from DSC and POM images viewed with a quarter-wave retardation plate indicate the presence of

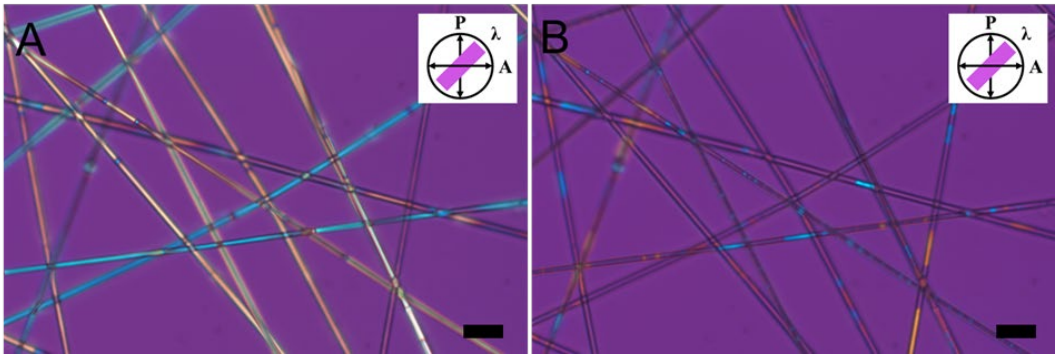

Figure 8. Crossed POM images with a quarter-wave retardation plate of fibers with 1.5 wt% **$C_4AzoC_6PEG_3$** at 25 °C before (*A*) and after (*B*) UV irradiation. Scale bars = 10 µm.

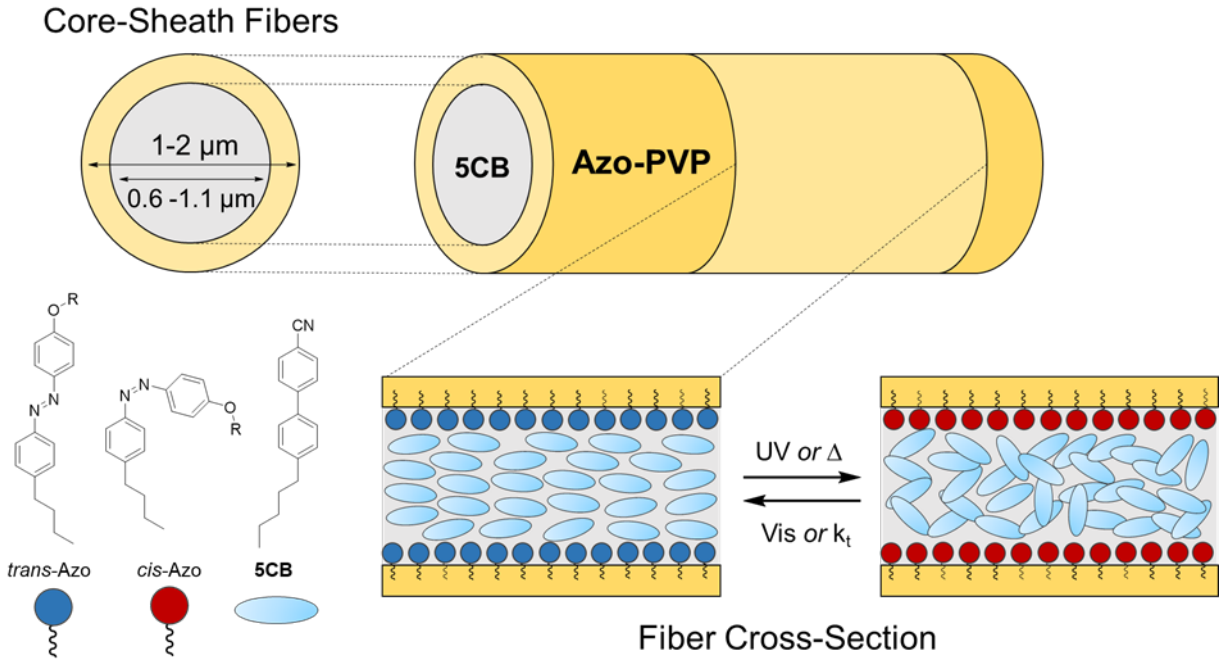

Scheme 1. An overview of the work presented in this system. Electrospun nanofibers are prepared with a PVP sheath doped with 0 – 3 wt% of an azobenzene-based surfactant and a neat **5CB** core. Irradiation of the nanofibers containing **$C_4AzoC_6PEG_3$** results in the disorder of the LC core and a depression of the N → I transition temperature which is reversible with visible light.

$C_4AzoC_6PEG_3$ at the polymer/LC interface has a significant affect on the LC ordering and alignmnet. With UV irradiaiton, these effects are amplified due to the presence of *cis*-**$C_4AzoC_6PEG_3$** at the LC/polymer and its incompatibility with the LC mesophase. With the disruption of the energy gained from surface anchoring, the bulk LC is unable to favorably align along any preferred axis leading to a disorganized core with nematic areas having no preferred orientation and significant areas appearing isotropic. Thus, the addition of **$C_4AzoC_6PEG_3$** into the polymer sheath is not only a means to photochemically control the optical properties of the LC core, but also serves as a facile method to modulate LC alignment within the fibers enabling the user to switch from LC fibers with strong planar axial alignment to those with random orientation using UV and visible light respectively. A general illustration of the observations presented in this work are given in Scheme 1.

In the absence of surfactant, or with low concentration of surfactant, the LC exhibits planar alignment along the fiber long axis. Irradiation of the nanofibers containing **$C_4AzoC_6PEG_3$** results in the disorder of the LC core and a depression of the $T_{N\rightarrow I}$, and at 3.0 wt% of **$C_4AzoC_6PEG_3$**, lowers the phase transition below room temperature. The decrease in $T_{N\rightarrow I}$ before irradiation was attributed to the disruption of the surface anchoring of the LC with increasing concentrations of **$C_4AzoC_6PEG_3$**. When in its *cis* isomer, the surfactant present at the LC/polymer interface is incompatible with the bulk LC leading to disorder of the confined LC core. Thus, the photochromic nature of the system suggests that the photochemical depression of the $T_{N\rightarrow I}$ is a result of the difference in the compatibility between the *cis* and *trans* isomers with the LC matrix present at the LC/polymer interface. Similar to "command surfaces" of Langmuir Blodgett films, the incorporation of azobenzene into the polymeric sheath of LC-

core nanofibers allows for control over the LC optical behavior by allowing for alignment and phase of the LC core to be controlled with light by controlling surface interactions at the interface.

Conclusions

We have shown that addition of an azobenzene-based photochromic surfactant (**$C_4AzoC_6PEG_3$**) into the polymer sheath of coaxially spun core-sheath LC-nanofibers results in the phase alignment, and thus the birefringence, of the nanofibers to be controlled photochemically. Cross-sectional images with FIB-SEM demonstrate that incorporation of **$C_4AzoC_6PEG_3$** into the polymer sheath does not affect the core-sheath integrity of the nanofibers. In the absence of surfactant, the LC exhibits planar alignment with the PVP sheath, but high concentrations of surfactant disrupt LC ordering due to surface interactions at the LC/PVP interface. The alignment can be modulated photochemically with UV irradiation inducing random alignment and visible irradiation restoring the planar axial orientation. This work broadens the range of applicability of electrospun LC nanofibers by varying the range of stimuli to affect the LC optical properties. The surfactant is used as a dopant in the polymer sheath as opposed to directly into the LC core, thus affecting LC properties by controlling surface interactions.

Author Contributions

The manuscript was written through contributions of all authors. All authors have given approval to the final version of the manuscript.

Conflicts of interest

There are no conflicts to declare.

Acknowledgements

This material is based upon work supported by the Office of Naval Research through the U.S. Naval Research Laboratory. M.D.T. acknowledges support from the American Society for Engineering Education.

Notes and references

1. K. Hiltrop and H. Stegemeyer, *Ber Bunsen Phys Chem*, 1981, **85**, 582-588.
2. F. C. Saunders, J. Staromlynska, G. W. Smith and M. F. Daniels, *Molecular Crystals and Liquid Crystals*, 1985, **122**, 297-308.
3. K. Choudhary, R. K. Gupta, R. Pratibha, B. K. Sadashiva and V. Manjuladevi, *Liquid Crystals*, 2019, **46**, 1494-1504.
4. K. Ariga, M. Nishikawa, T. Mori, J. Takeya, L. K. Shrestha and J. P. Hill, *Sci Technol Adv Mat*, 2019, **20**, 51-95.
5. H. Qi and T. Hegmann, *ACS Appl Mater Interfaces*, 2009, **1**, 1731-1738.
6. H. Qi, B. Kinkead, V. M. Marx, H. R. Zhang and T. Hegmann, *Chemphyschem*, 2009, **10**, 1211-1218.
7. B. Senyuk, J. S. Evans, P. J. Ackerman, T. Lee, P. Manna, L. Vigderman, E. R. Zubarev, J. van de Lagemaat and Smalyukh, II, *Nano Lett*, 2012, **12**, 955-963.
8. K. Ichimura, *Chem Rev*, 2000, **100**, 1847-1874.
9. H. K. Bisoyi and Q. Li, *Chem Rev*, 2016, **116**, 15089-15166.
10. S.-R. Keum, C.-H. Cho and Y.-K. Choi, *Dyes and Pigments*, 2004, **60**, 147-153.
11. T. Yamaguchi, T. Inagawa, H. Nakazumi, S. Irie and M. Irie, *Journal of Materials Chemistry*, 2001, **11**, 2453-2458.
12. V. Y. Chang, C. Fedele, A. Priimagi, A. Shishido and C. J. Barrett, *Advanced Optical Materials*, 2019, **7**.
13. G. S. Hartley, *Nature* 1937, **140**.
14. A. Natansohn and P. Rochon, *Chemical Reviews*, 2002, **102**, 4139-4175.
15. A. A. Beharry and G. A. Woolley, *Chem Soc Rev*, 2011, **40**, 4422-4437.
16. H. M. Bandara and S. C. Burdette, *Chem Soc Rev*, 2012, **41**, 1809-1825.
17. J. Garcia-Amoros and D. Velasco, *Beilstein J Org Chem*, 2012, **8**, 1003-1017.
18. I. C. Steven L. Murov, Gordon L. Hug, *Handbook of Photochemistry, Second Edition*, CRC Press, New York, New York, 1993.
19. T. Cusati, G. Granucci and M. Persico, *J Am Chem Soc*, 2011, **133**, 5109-5123.
20. L. Duarte, R. Fausto and I. Reva, *Physical Chemistry Chemical Physics*, 2014, **16**.
21. L. Vetrakova, V. Ladanyi, J. Al Anshori, P. Dvorak, J. Wirz and D. Heger, *Photochemical & Photobiological Sciences*, 2017, **16**, 1749-1756.
22. T. Ikeda, T. Sasaki and H. B. Kim, *J Phys Chem-Us*, 1991, **95**, 509-511.
23. T. Ikeda and O. Tsutsumi, *Science*, 1995, **268**, 1873-1875.
24. O. Tsutsumi, Y. Demachi, A. Kanazawa, T. Shiono, T. Ikeda and Y. Nagase, *Journal of Physical Chemistry B.* , 1998, **102**, 5.
25. O. Tsutsumi, A. Kanazawa, T. Shiono, T. Ikeda and L. Park, *Phys Chem Chem Phys*, 1999, **1**, 5.
26. J. H. Sung, S. Hirano, O. Tsutsumi, A. Kanazawa, T. Shiono and T. Ikeda, *Chemistry of Materials*, 2002, **14**, 385-391.
27. K. Ichimura, Y. Suzuki, T. Seki, A. Hosoki and K. Aoki, *Langmuir*, 1988, **4**, 1214-1216.
28. T. Seki, M. Sakuragi, Y. Kawanishi, Y. Suzuki, T. Tamaki, R. Fukuda and K. Ichimura, *Langmuir*, 1993, **9**, 211-218.
29. T. G. Shang, K. A. Smith and T. A. Hatton, *Langmuir*, 2003, **19**, 10764-10773.
30. B. A. Cicciarelli, T. A. Hatton and K. A. Smith, *Langmuir*, 2007, **23**, 4753-4764.
31. J. Sun, S. Hirano, O. Tsutsumi, A. Kanazawa, T. Shiono and T. Ikeda, *Chem. Mater.*, 2002, **14**, 7.
32. J. Garcia-Amoros, A. Szymczyk and D. Velasco, *Phys Chem Chem Phys*, 2009, **11**, 4244-4250.
33. J. E. Houston, E. A. Kelly, M. Kruteva, K. Chrissopoulou, N. Cowieson and R. C. Evans, *Journal of Materials Chemistry C*, 2019, **7**, 10945-10952.
34. Z. Y. Kuang, Y. J. Fan, L. Tao, M. L. Li, N. Zhao, P. Wang, E. Q. Chen, F. Fan and H. L. Xie, *Acs Appl Mater Inter*, 2018, **10**, 27269-27277.
35. S. H. Ryu and D. K. Yoon, *Liquid Crystals*, 2016, **43**, 1951-1972.

36. M. Urbanski, C. G. Reyes, J. Noh, A. Sharma, Y. Geng, V. Subba Rao Jampani and J. P. Lagerwall, *J Phys Condens Matter*, 2017, **29**, 133003.
37. J. P. Lagerwall, J. T. McCann, E. Formo, G. Scalia and Y. Xia, *Chem Commun (Camb)*, 2008, 5420-5422.
38. E. Enz, U. Baumeister and J. Lagerwall, *Beilstein J Org Chem*, 2009, **5**, 58.
39. Y. Kye, C. Kim and J. Lagerwall, *Journal of Materials Chemistry C*, 2015, **3**, 8979-8985.
40. M. J. Bertocchi, D. C. Ratchford, R. Casalini, J. H. Wynne and J. G. Lundin, *The Journal of Physical Chemistry C*, 2018, **122**, 16964-16973.
41. C. G. Reyes and J. P. F. Lagerwall, *ACS Appl Mater Interfaces*, 2020, **12**, 26566-26576.
42. J. Xue, T. Wu, Y. Dai and Y. Xia, *Chem Rev*, 2019, **119**, 5298-5415.
43. E. Enz and J. Lagerwall, *Journal of Materials Chemistry*, 2010, **20**.
44. J. Nguyen, R. M. Stwodah, C. L. Vasey, B. E. Rabatin, B. Atherton, P. A. D'Angelo, K. W. Swana and C. Tang, *Polymers (Basel)*, 2020, **12**.
45. C. G. Reyes, A. Sharma and J. P. F. Lagerwall, *Liquid Crystals*, 2016, **43**, 1986-2001.
46. L. Pschyklenk, T. Wagner, A. Lorenz and P. Kaul, *ACS Applied Polymer Materials*, 2020, **2**, 1925-1932.
47. J. D. Lin, C. P. Chen, L. J. Chen, Y. C. Chuang, S. Y. Huang and C. R. Lee, *Opt Express*, 2016, **24**, 3112-3126.
48. M. D. Thum, D. C. Ratchford, R. Casalini, J. H. Wynne and J. G. Lundin, *Acs Applied Nano Materials*, 2021, **4**, 297-304.
49. S. Talwar, A. S. Krishnan, J. P. Hinestroza, B. Pourdeyhimi and S. A. Khan, *Macromolecules*, 2010, **43**, 7650-7656.
50. K. T. Dicker, D. Ratchford, R. Casalini, M. D. Thum, J. H. Wynne and J. G. Lundin, *Langmuir*, 2020, **36**, 7916-7924.
51. G. P. Crawford, R. Ondris-Crawford, S. Zumer and J. W. Doane, *Phys Rev Lett*, 1993, **70**, 1838-1841.
52. S. Santiago, P. Gimenez-Gomez, X. Munoz-Berbel, J. Hernando and G. Guirado, *ACS Appl Mater Interfaces*, 2021, **13**, 26461-26471.
53. M. Mariello, A. Qualtieri, G. Mele and M. De Vittorio, *ACS Appl Mater Interfaces*, 2021, **13**, 20606-20621.
54. Z. Niu and W. Yuan, *ACS Appl Mater Interfaces*, 2021, **13**, 4508-4518.
55. Y. Xing, Y. M. Xu, Q. L. Wu, G. Wang and M. F. Zhu, *Journal of Materials Chemistry C*, 2021, **9**, 439-455.
56. G. M. Kehe, D. I. Mori, M. J. Schurr and D. P. Nair, *ACS Appl Mater Interfaces*, 2019, **11**, 1760-1765.
57. D. P. Ura, J. Knapczyk-Korczak, P. K. Szewczyk, E. A. Sroczyk, T. Busolo, M. M. Marzec, A. Bernasik, S. Kar-Narayan and U. Stachewicz, *ACS Nano*, 2021, **15**, 8848-8859.
58. B. J. Ku, B. M. Lee, D. H. Kim, A. Mnoyan, S. K. Hong, K. S. Go, E. H. Kwon, S. H. Kim, J. H. Choi and K. Lee, *ACS Appl Mater Interfaces*, 2021, **13**, 13106-13113.
59. J. Garcia-Amoros, G. Stopa, G. Stochel, R. van Eldik, M. Martinez and D. Velasco, *Phys Chem Chem Phys*, 2018, **20**, 1286-1292.